Talanta 284 (2025) 127182

Contents lists available at ScienceDirect

Talanta

journal homepage: www.elsevier.com/locate/talanta

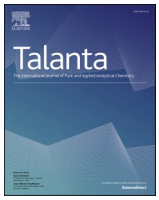

# Tetrahedral DNA nanostructures, graphene and carbon nanodots-based electrochemiluminescent biosensor for BRCA1 gene mutation detection

Daniel García-Fernández [a], Laura Gutiérrez-Gálvez [a], David López-Diego [b], Mónica Luna [b], Íñigo Torres [c], Félix Zamora [c,d], Jesús Solera [f], Tania García-Mendiola [a,d,*], Encarnación Lorenzo [a,d,e]

[a] Departamento de Química Analítica y Análisis Instrumental, Universidad Autónoma de Madrid, 28049, Madrid, Spain
[b] Instituto de Micro y Nanotecnología IMN-CNM. CSIC (CEI UAM+CSIC), 28760, Tres Cantos, Madrid, Spain
[c] Departamento de Química Inorgánica and Condensed Matter Physics Center (IFIMAC), Universidad Autónoma de Madrid. 28049, Madrid Spain
[d] Institute for Advanced Research in Chemical Sciences (IAdChem), Universidad Autónoma de Madrid, 28049, Madrid, Spain
[e] IMDEA-Nanociencia, Ciudad Universitaria de Cantoblanco, 28049, Madrid, Spain
[f] Molecular Oncogenetics Unit, La Paz Universitary Hospital, Biochemistry Department, Faculty of Medicine, Universidad Autónoma de Madrid, Madrid 28046, Spain

ARTICLE INFO

*Keywords:*
DNA biosensor
Electrochemiluminescence (ECL)
Breast cancer type 1 (BRCA1) gene
Carbon nanodots (CNDs)
Tetrahedral DNA nanostructures (TDNs)

ABSTRACT

In this study, we present a novel electrochemiluminescent DNA biosensor designed for detecting breast cancer type 1 (BRCA1) gene mutations. The biosensor integrates graphene nanosheets (Graph-NS), tetrahedral DNA nanostructures (TDNs), and carbon nanodots (CNDs) to enhance sensitivity and specificity. Graph-NS are employed to structure the transducer and serve as a platform for DNA immobilization. TDNs are engineered with a BRCA1 gene-specific capture probe located at the apex (TDN-BRCA1), facilitating efficient biorecognition. Additionally, the basal vertices of TDNs are functionalized with amino groups, enabling their attachment to the CSPE/Graph-NS surface via amino-graphene interaction. This platform effectively identifies single-base mutations in the BRCA1 gene utilizing synthesized CNDs as a coreactant and $[Ru(bpy)_3]^{2+}$ as the luminophore through the coreactant pathway. The developed biosensor demonstrates exceptional sensitivity and can detect a single mutation in the BRCA1 gene. Furthermore, it has been successfully validated in real samples obtained from breast cancer patients, showcasing a remarkable detection limit of 1.41 aM.

## 1. Introduction

Breast cancer became the most common type of cancer in females, accounting for 31 % of female cancers and also becoming the second leading cause of death in middle-aged women [1,2]. During the last decade, there has been a significant increase in breast cancer cases, whilst the tendency on estimated deaths caused by this disease is dropping lower (https://seer.cancer.gov/Last checked: May 2024). Early diagnosis helps maintain this statistic since the best prognosis is acquired when breast cancer is diagnosed at an early phase [3]. Among all inherited breast cancers, it is estimated that mutations in the breast cancer type cause 80 % of them, susceptibility protein gene (BRCA1), a tumour suppressor biomarker [4]. Currently, the lack of reliable, low-cost and easy-to-use devices to detect breast cancer at an early stage raises the morbidity rate to 80 % in some regions [5]. Most of the diagnosis techniques for breast cancer are laborious, expensive, and need highly trained specialists, thus, the methods are pretty unpractical [6]. Consequently, it is of great interest to develop new breast cancer gene mutation detection methods with greater efficiency that present fewer limitations than the current methodologies.

In this sense, biosensors are presented as alternative tools to detect gene mutations since they have advantages, including high sensitivity, rapidity, adaptability, easiness of use and preparation and possibility of miniaturization [7]. Considering the used biorecognition element, biosensors can be classified into different categories. Specifically, a DNA biosensor is developed when the biorecognition element is a DNA probe. This biosensor provides advantages such as high selectivity, low cost, and user-friendly nature; therefore, different DNA biosensors for BRCA1 detection have been developed. This technology opens the door for the development of new rapid, simple, and low-cost sensing platforms for biomarker detection as an alternative to the traditional techniques that are currently used. However, some works described in the literature

* Corresponding author. Departamento de Química Analítica y Análisis Instrumental, Universidad Autónoma de Madrid, 28049, Madrid, Spain.
*E-mail address:* tania.garcia@uam.es (T. García-Mendiola).

https://doi.org/10.1016/j.talanta.2024.127182
Received 20 August 2024; Received in revised form 23 October 2024; Accepted 6 November 2024
Available online 10 November 2024

**Table 1**
DNA oligonucleotides used in this work.

| | Oligonucleotide sequence | Named |
|---|---|---|
| BRCA1 probe | 5'- $NH_2$- GAC TCA CCT GCA ATA AGT TG | BRCA1-Probe |
| Tetra-A-PROBE-BRCA1 | 5'-GAC TCA CCT GCA ATA AGT TG TTTTTTTTTT ACA TTC CTA AGT CTG AAA CAT TAC AGC TTG CTA CAC GAG AAG AGC CGC CAT AGT A-3' | Tetra-A-BRCA1 |
| Tetra-B | 5'-$NH_2$-TAT CAC CAG GCA GTT GAC AGT GTA GCA AGC TGT AAT AGA TGC GAG GGT CCA ATA C-3' | Tetra-B |
| Tetra-C | 5'- $NH_2$-TCA ACT GCC TGG TGA TAA AAC GAC ACT ACG TGG GAA TCT ACT ATG GCG GCT CTT C-3' | Tetra-C |
| Tetra-D | 5'- $NH_2$-TTC AGA CTT AGG AAT GTG CTT CCC ACG TAG TGT CGT TTG TAT TGG ACC CTC GCA T-3' | Tetra-D |
| Complementary synthetic sequence for BRCA1 probe | 5'- CTG AGT GGA CGT TAT TCA AC -3' | BRCA1-C |
| Mutated synthetic sequence for BRCA1 probe | 5'- CTG AGT GGA TGT TAT TCA AC -3' | BRCA1-M |
| Non-complementary sequence for BRCA1 probe | 5'-CCA GGT GGA ACA TCA TCC GGT GAT GC-3' | BRCA1-NC |

recently [8–10] present some drawbacks as low sensitivity, complex development, etc. Thus, in this work, the development of an innovative DNA biosensor for sensitive breast cancer biomarker cancer detection is proposed.

DNA biosensors may be classified through their transduction mechanisms, among them, electrochemiluminescence (ECL) has drawn the attention of the scientific community. ECL can be considered a combination of electrochemical and optical methods, offering specific advantages over chemiluminescence and photoluminescence, such as high sensitivity or low background noise due to the absence of excitation light sources [11]. ECL is a process in which species produced at an electrode undergo high-energy electron transfer reactions, reaching excited states that emit light as they return to their ground state. Thus, ECL has become a fascinating analytical technique that is applied in all kinds of fields, such as immunoassays, environmental studies, and bioanalysis, due to its wide dynamic range, high sensitivity, and excellent reliability [12–15].

This excited state can be achieved through two different pathways: the ion annihilation pathway and the coreactant pathway since it is advantageous when the radical species are not stable enough to operate according to the ion annihilation pathway or when the used solvents have a narrow potential window that does not allow the formation of radical ions [16]. Moreover, this mechanism may lead to more intense ECL signals and can eradicate quenching effects [17].

Nowadays, most ECL applications involve the coreactant ECL system. Most commonly the system based on the use of $[Ru(bpy)_3]^{2+}$ as the luminophore and tripropylamine (TPrA) as the coreactant [18]. Lately, new alternatives to TPrA have been being used since this amine brings up some drawbacks due to its toxicity, volatility, and low sensitivity. Therefore, the necessity of finding new coreactants for biological assays was found. Lately, carbon nanodots (CNDs) have appeared as a possible solution due to their outstanding properties, including facile synthesis, low toxicity, tuneable fluorescence emission, inertness to chemicals, aqueous dispersibility, biocompatibility, great optical properties, and ease of functionalization [19,20].

Recently, nanomaterials have brought attention to biosensors' development due to their positive inputs for their analytical properties. In this sense, graphene has caught the scientific community's attention for the last decade. Graphene is a single-layer carbon allotrope with hexagonally arranged atoms [21]. This nanomaterial supplies advantages like easy and low-cost synthesis, ease of functionalization, water dispersibility and high electrical conductivity [22], becoming a perfect choice as a biosensor transducer. Also, it can be functionalized with biomolecules through the amino-graphene interaction [23], which is an attractive nanomaterial in biosensor design.

One of the most essential stages in DNA biosensor development is immobilizing the biological element. In this sense, DNA nanostructures based on probe self-assembly have gained prominence due to their programmability and specificity. DNA self-assembly relies on the pairing of nitrogenous bases, allowing oligonucleotides to serve as "building materials" independent of their genetic information. One widely used method is DNA Origami, developed by [24], which involves folding a long single-strand viral DNA (scaffold) into the desired structure with the help of short DNA fragments (staples). This method requires intricate design and preparation, prompting the development of new approaches such as the synthesis of three-dimensional polyhedral DNA nanostructures. These structures, constructed through the base complementarity of short single-stranded DNA, have garnered significant scientific interest [25]. Among these, tetrahedral DNA nanostructures have emerged as a particularly promising alternative in the field of biosensing due to their advantageous properties [26].

A new challenge is the necessity to build novel biosensing platforms; these nanostructures can be designed and functionalized with biomolecules during the production process. Recent discoveries have revealed that tetrahedral DNA nanostructures functionalized with capture probes offer significant advantages for improving biomolecular recognition on bioassay platforms [27]. These advantages stem from the well-defined spacing between probes, increased stability of tetrahedral DNA nanostructures compared to traditional strategies and the specific orientation.

Considering the above described and to improve analytical performance in DNA biosensors, the development of a new electrochemiluminescent DNA biosensor for BRCA1 gene mutation detection based on combining tetrahedral DNA nanostructures (TDNs), graphene

**Table 2**
Clinical samples from breast cancer patients. All patients signed an informed consent approved by the ethics committee of the Hospital Universitario "La Paz".

| | Oligonucleotide sequence | Named |
|---|---|---|
| Complementary sequence(control) | TGATTTTAAACTATAATTTTTGCAGAATGTGAAA<br>AGCTATTTTTCCAATCATGATGAAAGTCTGAAGA<br>AAAATGATAGATTTATCGCTTCTGTGACAGACA<br>GTGAAAACACAAATCAAAGAGAAGCTGCAAGTC<br>ATGGTAAGTCCTCTGTTTAGTTGAACTA | WT |
| Mutated sequence | TGATTTTAAACTATAATTTTTGCAGAATGTGAAA<br>AGCTATTTTTCCAATCATGATGAAAAGTCTGAAGA<br>AAAATGATAGATTTATCGCTTCTGTGACAGACAGTG<br>AAAACACAAATCAAAGAGAAGCTGCAAGTCATGGTA<br>AGTCCTCTGTTTAGTTGAACTA | MUT |

nanosheets (Graph-NS) and CNDs is proposed.

## 2. Materials and methods

### 2.1. Chemicals

Sodium phosphate dibasic dihydrate ($Na_2HPO_4{\cdot}2H_2O$), sodium phosphate monobasic monohydrate ($NaH_2PO_4{\cdot}H_2O$), sodium chloride (NaCl), tris(hydroxymethyl)aminomethane (Tris, $NH_2C(CH_2OH)_3$), and hydrochloric acid (HCl), sodium hydroxide (NaOH) and magnesium chloride ($MgCl_2$) were purchased from Merck. Graphite powder (flake size <150 μm) was purchased from Aldrich. Methanol was purchased from Scharlab. Tigernut milk was purchased from Mercadona Co. a Spanish supermarket.

DNA oligonucleotides (Table 1) were also purchased from Merck. The designs of Tetra-A, Tetra-B, Tetra-C, and Tetra-D were previously reported by Pei et al. (2010). In these designs, the red regions indicate the capture probe and, also, the analyte (complementary strand), the other coloured regions represent the building regions of the nano-tetrahedron scaffold through base complementarity. Additionally, the mutated nitrogenous base in the mutated strand (BRCA1-M) is marked in green.

Clinical samples of the BRCA1 gene from exon 9, including both wild type (WT) and mutated (MUT) forms, were provided and verified by Dr. Jesús Solera from La Paz Hospital in Madrid, Spain, and are listed in Table 2. The BRCA1 mutation involves the insertion of an adenine nucleotide, which is highlighted in red in the sequence.

### 2.2. Apparatus

For fluorescent measurements, a Varian Cary Eclipse spectrofluorometer and quartz cuvettes with an optical path of 1.00 cm were used.

For UV–Visible spectrum measurements, a PharmaSpec UV-1700 series spectrophotometer (Shimadzu Corporation) and quartz cuvettes with an optical path of 1.00 cm were used. Spectra were recorded in a range of 200–800 nm.

TDNs were synthetized using a MiniAmpPlus™ Thermal Cycler.

All solutions were prepared with Milli-Q water, obtained from a purified water Millipore Milli-Q System (18.2 MΩ cm). Solutions and materials wer sterilized using a Nüve OT012 autoclave.

Electrochemiluminescence (ECL) was measured by using a SpectroECL from Metrohm DropSens controlled with DropView SPELEC software. The instrument combines a bipotentiostat/galvanostat (±4 V potential range, ±40 mA maximum measurable current). A Metrohm DropSens Si-photodiode cell (DRP-ECLPHOTODIODCELL), with a spectral response range of 340–1100 nm was used. Carbon screen-printed electrodes (CSPE) were purchased from Metrohm.

Atomic Force Microscopy (AFM) images were acquired with a Nanotec Electrónica AFM system. WSxM software [28] was used for the acquisition and processing of images.

SEM-EDAX analysis was performed with a VERIOS 460 microscope from FEI.

### 2.3. Procedures

#### 2.3.1. Carbon nanodots synthesis

Carbon nanodots (CNDs) were synthesized using a green chemistry approach that involved the carbonization of tigernut milk via a microwave-assisted hydrothermal treatment, following an optimized procedure previously reported by us [14,29,30]. Briefly, 3.00 mL of tigernut milk was placed in a quartz flask and subjected to optimized microwave-assisted hydrothermal treatment (30 min, 200 °C, 50 W, and 170 psi) under magnetic stirring in a microwave reactor synthesizer. Once the resulting solution cooled to room temperature, it was purified by filtration (0.45 μm nylon syringe filter) and dialyzed for 1.5 h (Spectra/Por® 6 membrane, MWCO 1 kDa, supplied by SGL). Finally, the CNDs solution was stored at 4 °C, protected from light.

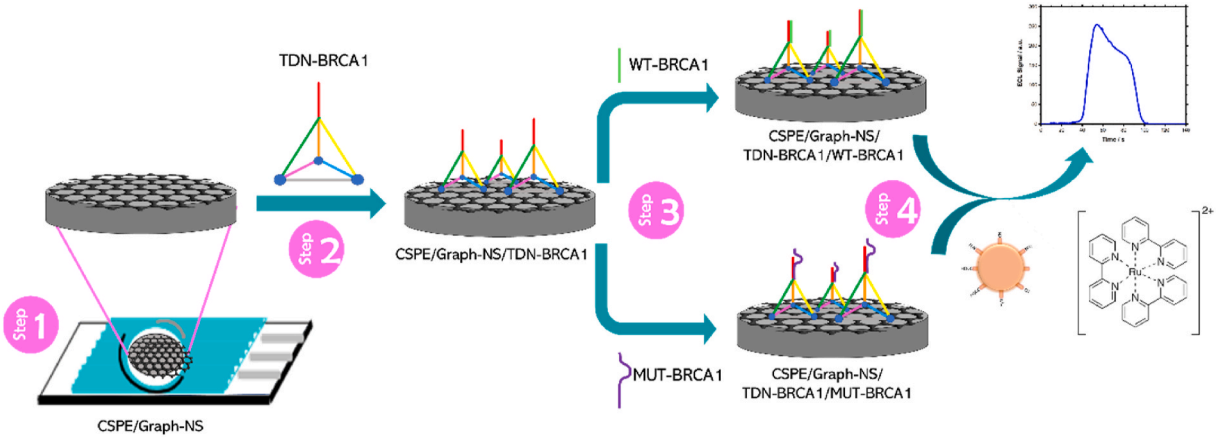


**Scheme 1.** BRCA1 gene ECL biosensor development.

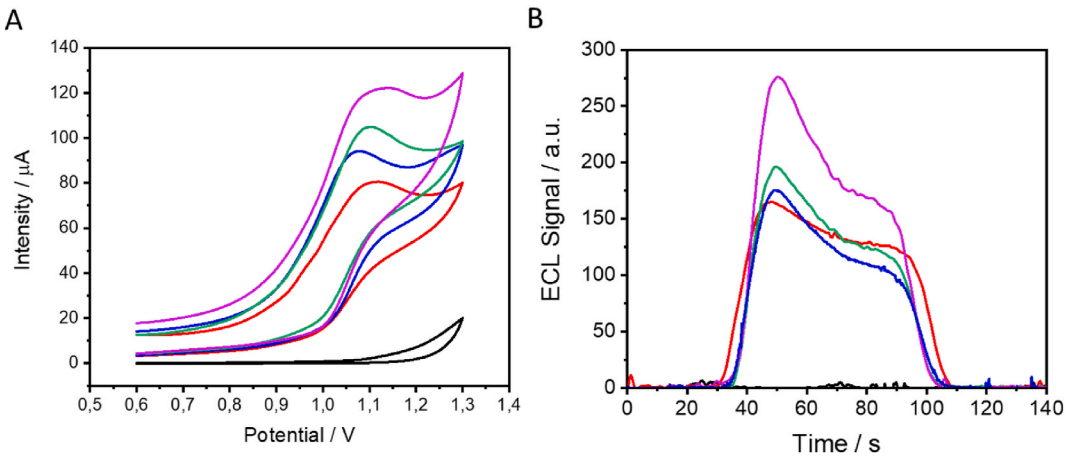


**Fig. 1. (A)** Cyclic voltammograms and **(B)** ECL signals of: CSPE in a solution of 75 μL of PB 0.1 M pH = 8.0 (**black line**), CSPE in a solution of $[Ru(bpy)_3]^{2+}$ 7 mM and CNDs (**red line**), CSPE/Graph-NS in a solution of $[Ru(bpy)_3]^{2+}$ 7 mM and CNDs (**blue line**); CSPE/Graph-NS/TDN in a solution of $[Ru(bpy)_3]^{2+}$ 7 mM and CNDs (**green line**) and CSPE/Graph-NS/TDN/BRCA1-C in a solution of $[Ru(bpy)_3]^{2+}$ 7 mM and CNDs (**purple line**).

### 2.3.2. Graphene nanosheets synthesis

Graphene nanosheets (Graph-NS) were synthesized in two steps. Firstly, 100 mg of graphite powder from Aldrich (flake size <150 μm) were put into a 20 mL ball milling reactor with 30 stainless steel balls. The powder was milled for 180 min at 3000 rpm. After that, 25 mg of the ball-milled graphite were put, with 10 mL of methanol on a 20 mL vial. The mixture was exfoliated with a shear-mixer device for 90 min at 25000 rpm. Then, the obtained black suspension was centrifuged at 4500 rpm (1900 rcf) for 60 min and the clear supernatant was recovered achieving a concentration of 0,015 g $L^{-1}$.

### 2.3.3. Oligonucleotides preparation

Stock solution of aminated BRCA1-PROBE was reconstituted with phosphate buffer 10 mM at pH = 7.0 (PB) at a concentration of 100 μM. Stock solutions of the TDN (Tetra-A-BRCA1, Tetra-B, Tetra-C and Tetra-D) were reconstituted with previously sterilized Milli-Q water at a concentration of 100 μM with sterilized purified Milli-Q water. Stock solutions of the non-aminated oligonucleotides (BRCA1-C, BRCA1-M and BRCA1-NC) were reconstituted with phosphate buffer 10 mM, 0.4 M NaCl at pH = 7.0 (PBS) at a concentration of 100 μM. From these solutions, aliquots of 100 μL were prepared and stored in a freezer at −20 °C.

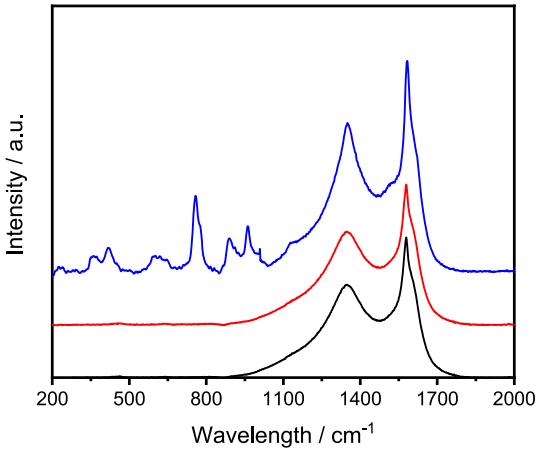


**Fig. 2.** Raman spectra for CSPE (**black curve**), CSPE/Graph-NS (**red curve**) and CSPE/Graph-NS/TDN (**blue curve**).

### 2.4. Tetrahedral DNA nanostructures synthesis

The previously mentioned oligonucleotides (Tetra-A-BRCA1, Tetra-B, C and D; see Table 1) were mixed in equimolar quantities in buffer 20 mM Tris 50 mM $MgCl_2$ pH 8.0 (TM Buffer). This mixture was then subjected to a thermocycler with a treatment divided into three stages, each consisting of steps lasting 2 min. The first stage included two steps at 95 °C and 51 °C; the second stage had four steps at 46.1 °C, 43.6 °C, 41.2 °C and 38.8 °C; and final stage had two steps of 30 °C and 4 °C.

### 2.4.1. BRCA1 gene biosensor preparation

Firstly, carbon screen-printed electrodes (CSPEs) were nanostructured by adsorption of 10.0 μL of graphene nanosheets (0.015 g $L^{-1}$) in methanol, which had been previously exfoliated through sonication to avoid aggregation, ensuring the homogeneity of the dispersion. To ensure the rapid evaporation of the methanol, the drop-casting process was done over a hot plate at 50 °C. Afterward, the electrodes were let to cool down to room temperature. These modified electrodes (CSPE/Graph-NS) were then incubated overnight with 10.0 μL of 1.00 μM TDNs which carry the BRCA1 gene capture probe (TDN-BRCA1). After that, to remove non-specific adsorbed materials, a washing step with Milli-Q sterilized water was carried out. The modified electrode (CSPE/Graph-NS/TDN-BRCA1) was incubated for an hour at 38 °C with 10.0 μL of the analyte solution (BRCA1-C) with an adequate concentration. Again, a second washing step was carried out. The obtained platform (CSPE/Graph-NS/TDN-BRCA1/BRCA1-C) was then ready for ECL signal measurement.

### 2.5. Biosensor characterization

AFM images were acquired using silicon cantilevers in jumping mode (2.8 N/m nominal spring constant and 75 kHz resonant frequency in air, PPP-FM Nanosensors).

SEM images were obtained working on a low voltage (2 kV) and current (13 pA) mode to minimize the damage to the samples. The EDAX spectra resolution was 127 eV.

### 2.6. Electrochemiluminescence measurements

60.0 μL of a $Ru[(bpy)_3]^{2+}$ and CNDs solution on phosphate buffer at pH = 8.0 were added over the biosensor platform. ECL signal was then acquired by applying a cyclic potential scan from 0.60 V to 1.30 V at a scan rate of 10 mV/s and an optical amplification of 10x. The resulting cyclic voltammogram and ECL signal were recorded simultaneously.

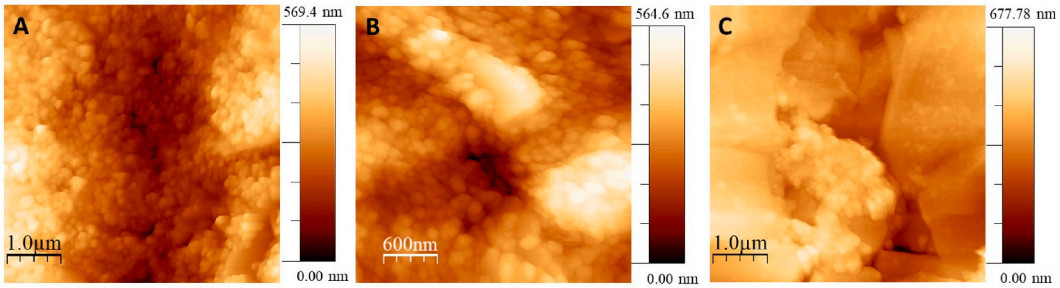


**Fig. 3.** Topographical AFM images of CSPE (A), CSPE/Graph-NS (B), and CSPE/Graph-NS/TDN (C) on $SiO_2$.

### *2.7. DNA Extraction and purification from peripheral blood samples and PCR amplification*

All patients signed a study informed consent form, approved by the Hospital Universitario La Paz ethical committee. Clinical samples of genomic DNA employed were obtained from patient's peripheral blood cells using a DNA Blood kit (Qiagen, Spain) and the Chemagen platform (PerkinElmer, Spain) following the manufacturers' instructions. All coding exons were analyzed to detect any potential mutations in the BRCA1 gene. The analysis began with PCR amplification of each canonical exon using oligonucleotides that anneal to the flanking introns. Each amplicon was analyzed by agarose gel electrophoresis, and all PCR products were sequenced using Sanger sequencing on an ABI 3730 DNA analyzer (ThermoFisher Scientific). Additionally, multiplex ligation-dependent probe amplification (MLPA) was conducted to identify any genomic deletions or duplications using SALA MLPA Probemix P002 kits (MRC-Holland), according to the manufacturers' instructions. The clinical samples included both wild type (WT) and mutated (MUT) forms of the BRCA1 gene.

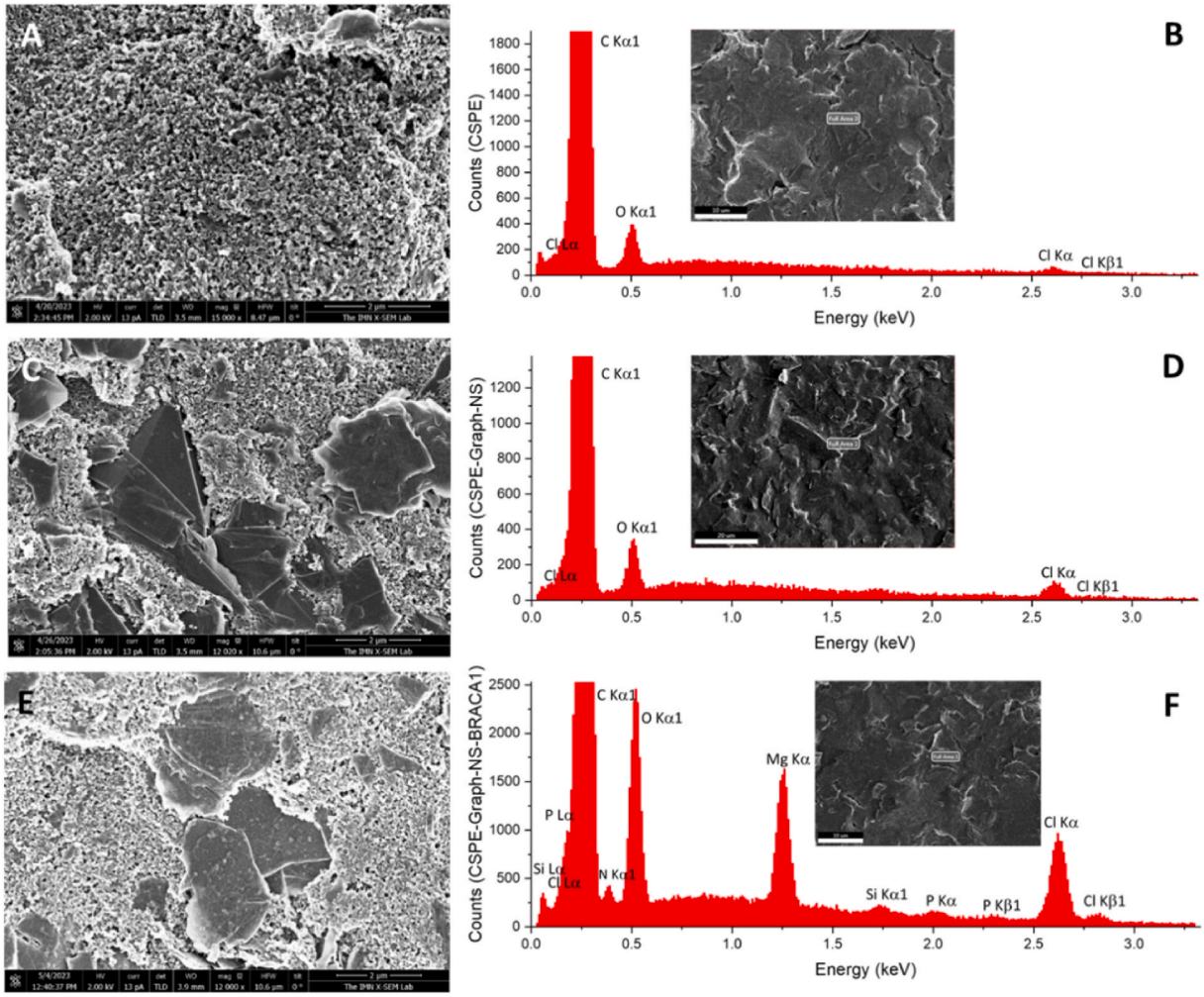


**Fig. 4.** Secondary electron SEM images (A, C, E) and EDAX analysis (B, D, F) of CSPE (A, B), CSPE/Graph-NS (C, D) and CSPE/Graph-NS/TDN (E, F). Graphene sheets can be clearly visualized on the surface of the modified CSPE samples (CSPE/Graph-NS (C) and CSPE/Graph-NS/TDN (E)). The EDAX peaks corresponding to the energy of Phosphorus are only detected on the CSPE/Graph-NS/TDN sample (F). The inset images on the EDAX spectra show the area analyzed. For each spectrum, the plotting was limited to 1/12 of the maximum counts of its carbon peak in order to distinguish the details of the lesser counts peaks.

## 3. Results and discussions

Recently, we reported the use of the $[Ru[(bpy)_3]^{2+}$/CNDs electrochemiluminescence (ECL) system in biosensors [14,29,30].Building on these successful studies, the present research aims to take the next step by using the $[Ru[(bpy)_3]^{2+}$/CNDs ECL system in combination with graphene nanosheets (Graph-NS) and tetrahedral DNA nanostructures (TDNs) to detect highly specific hybridization event. As demonstrated in our previous works [14,29,30] we proposed an "oxidative-reduction" coreactant ECL pathway for the $[Ru[(bpy)_3]^{2+}$/CNDs system, as illustrated in the inset on Fig. S1A. As can be observed in Fig. S1B, $[Ru(bpy)_3]^{2+}$ shows the expected reversible redox process of $[Ru(bpy)_3]^{3+}/[Ru(bpy)_3]^{2+}$ system in its cyclic voltammogram while CNDs show an oxidation process around to 1.15 V (see ampliation on Figure S1B). None of them provide any ECL signal (Fig. S1A). When the system is evaluated ($[Ru(bpy)_3]^{2+}$/CNDs), the intensity of the $[Ru(bpy)_3]^{2+}$ oxidation peak increases concomitantly as the cathodic peak decreases (phenomenon characteristic of an electrocatalytic process) and an increasing ECL signal can be observed (Fig. S1A). These results suggest that CNDs act as coreactants in the anodic ECL of $[Ru(bpy)_3]^{2+}$, confirming the "oxidative–reduction" coreactant ECL mechanism for the $[Ru(bpy)_3]^{2+}$/CNDs system [14,29]. In this mechanism, $[Ru(bpy)_3]^{2+}$ is oxidized during the anodic scan. CNDs can be oxidized by the direct electro-oxidation of the nanomaterial (see inset of Figure S1A) and by via chemical oxidation of the oxygen-containing units by electrogenerated $[Ru(bpy)_3]^{3+}$ ($[Ru(bpy)_3]^{3+} + CDs \rightarrow [Ru(bpy)_3]^{2+} + CDs^{+\cdot}$) [31]. After that, oxidized CNDs ($CNDs^{+\cdot}$) undergoes chemical decomposition, forming the related reducing species ($CNDs^{\cdot}$) that subsequently reduces $[Ru(bpy)_3]^{3+}$ forming $[Ru(bpy)_3]^{2+*}$, which decays to the ground state generating an anodic red ECL emission [30].

Thus, in this work, a $Ru[(bpy)_3]^{2+}$/CNDs ECL biosensor is proposed and improved through the use of different nanomaterials such as graphene nanosheets (Graph-NS) and tetrahedral DNA nanostructures (TDNs). Therefore, this work's first step will focus on synthesizing and characterizing the three different nanomaterials.

### 3.1. Synthesis and characterization of CNDs

Carbon nanodots (CNDs) were synthesized using a green-chemistry approach involving the carbonization of tigernut milk. This process utilized an optimized microwave-assisted hydrothermal treatment, following a method that we have previously reported in the literature [14,29,30]. Thanks to the characterization studies (see Fig. S2), we have corroborated that the obtained nanoparticles present a quasi-spherical shape with an average size of (7.2 ± 1.4) nm. Their composition and functional groups of the surface were confirmed by elemental analysis and infrared absorption spectroscopy. Moreover, the presence of carboxylate groups on their surface was corroborated by zeta potential measurements since a negative average value in aqueous solution was obtained (-6.7 ± 0.3 mV) [30].

### 3.2. Synthesis and characterization of graphene nanosheets

The synthesis of Graph-NS followed a two-step procedure. Initially, commercial graphite powder was milled into a ball milling reactor with stainless steel balls. Subsequently, the ball-milled graphite was mixtured with methanol and exfoliated via a shear-mixer device for 90 min at 25000 rpm. Following this, the resulting dark suspension was centrifugated to obtain a clear suspension of Graph-NS. These nanosheets were analyzed by microscopic techniques such as and scanning electron microscopy (SEM) and transmission electron microscopy (TEM). Both techniques reveal the sharp-edge morphology of the Graph-NS which present dimensions between 100 and 500 nm (Figs. S3A–B). Additionally, the thickness of the nanosheets was analyzed by atomic force microscopy (AFM), presenting heights between 5 and 20 nm (Fig. S3C). The Raman spectrum of the nanosheets shows the D and D' bands centred on ~1350 $cm^{-1}$ and 1620 $cm^{-1}$ respectively, the G peak at ~1580 $cm^{-1}$ and, the 2D peak around ~2720 $cm^{-1}$ which are the characteristic signatures of few-layer graphene [32] (Fig. S4A). Moreover, a Raman mapping image was obtained integrating the G peak confirming the morphology observed in the microscopic techniques (Fig. S4B).

### 3.3. Synthesis and characterization of tetrahedral DNA nanostructures

The tetrahedral DNA nanostructures (TDNs) were assembled using three aminated 55-base oligonucleotides (Tetra-B, Tetra-C and Tetra-D) along with an 85-nucleotide strand (Tetra-A-BRCA1) that includes the DNA capture probe. This design incorporates a DNA capture probe at the 5′-end, complementary to a specific BRCA1 gene region. Each oligonucleotide forms one of the four tetrahedron faces (Fig. S5A), with 17-base pair segments that are complementary to those on the other three strands, indicated by matching colors in Fig. S5A and Table 1. The BRCA1 capture probe is positioned at one vertex (TDN-BRCA1) for hybridization with the target DNA, while the remaining three vertices feature amino groups for anchoring to the graphene nanosheet surface.

Existing TDN synthesis methods [27,33–36]; often neglect the risk of forming random structures. We developed an improved synthesis method involving a gradual and controlled temperature decrease, based on the melting temperatures (Tm) of each complementary fragment to ensure accurate hybridization and prevent undesired formations.

The melting temperature of every fragment used in the TDN synthesis was obtained using the formula $T_m = 64.9 + 41 \cdot (G + C - 16.4)/L$ [37], where G and C are the counts of guanine and cytosine bases in the sequence, and L is the number of bases (i.e. 17). These Tm values guided the synthesis procedure outlined in the materials and methods section.

To confirm the efficacy of our synthesis method, we used electrophoretic analysis, cryogenic electron microscopy (cryo-EM), and optical microscopy (bright-field and fluorescence).

Gel electrophoresis results (Fig. S5B) showed that TDN-ORF (lane 5) migrated slower than individual single-stranded DNA oligonucleotides (lanes 1 to 4) or trimer combinations missing one strand (lanes 6 to 9), indicating successful TDN-ORF synthesis [38]. These results were corroborated by cryo-EM images of TDN (Fig. S5D).

Bright-field and fluorescence microscopy used FAM-labelled TDN-ORF (TDN-ORF-FAM), synthesized with a Tetra-A sequence which carries, not only the ORF1ab capture probe but the FAM fluorophore (Tetra-A-ORF-FAM; see Table 1). Fig. S5C presents images of TDN-ORF-FAM on gold screen-printed electrodes, where the observed fluorescence from the FAM molecule attached to the TDN confirms successful synthesis and anchoring on the gold surface.

In summary, the TDN structure features a capture probe at one vertex for biorecognition, while the other three aminated vertices are prepared for graphene nanosheet surface modification.

### 3.4. BRCA1 gene ECL biosensor design

The biosensor was prepared following four basic steps described in Scheme 1. In the first step, CSPEs were modified with the Graph-NS solution. Over this nanostructured surface (CSPE/Graph-NS), tetrahedral DNA nanostructures containing the BRCA1 gene capture probe (TDN-BRCA1) were immobilized. After finishing this second step, the obtained platform (CSPE/Graph-NS/TDN-BRCA1) was incubated with the analyte (BRCA1-C), the BRCA1 gene (step 3). Finally, once the biorecognition reaction was carried out, the final platform was obtained (CSPE/Graph-NS/TDN-BRCA1/BRCA1-C), and a final ECL measurement step was done after adding an equimolar $[Ru(bpy)_3]^{2+}$/CNDs solution. Thus, the biosensor transduction was obtained through an ECL signal of $[Ru(bpy)_3]^{2+}$/CNDs by applying a cyclic potential scan to the electrode (step 4).

The following steps regarding the biosensor preparation were characterized through different techniques to confirm the correct

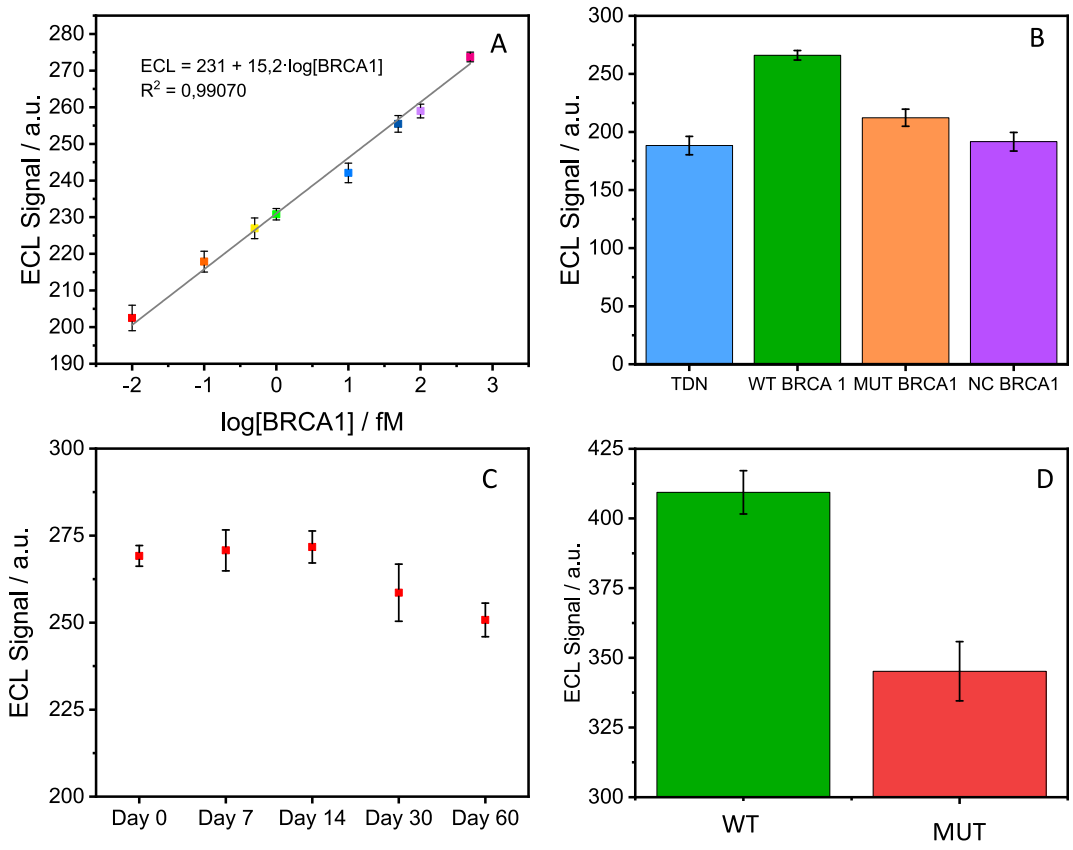


**Fig. 5.** (A) Calibration plot obtained through measurement of ECL signal of the nanostructured bioconjugate after hybridization with increasing amounts of BRCA1-C (red 10.0 aM, orange 100 aM, yellow 500 aM, green 1.00 fM, blue 10.0 fM, dark blue 100 fM, purple 500 fM and Pink 1.00 pM) (B) ECL signal obtained of the nanostructured bioconjugate before being challenged (blue bar) with (BRCA1-C 500 fM, green bar; BRCA1-M 500 fM, orange bar and NC BRCA1 500 fM, purple bar) (C) Nanostructured bioconjugate response to BRCA1-C 500 fM for 60 days. (D) Biosensor response to human serum samples of a negative $BRCA_1$ patient (green bar) and a BRCA1 patient (red bar).

preparation of the platform. Firstly, both electrochemical and electrochemiluminescent signals were registered at every step during biosensor development. As shown in Fig. 1A, the bare CSPE (black line) electrochemical signal is null. The following signals were measured, incubating with a solution of CNDs and $[Ru(bpy)_3]^{2+}$ to reach a closer approach to the designed experimental conditions for BRCA1 gene detection. The red line corresponds to the bare CSPE, and when incubated with CNDs and $[Ru(bpy)_3]^{2+}$, a shallow electrochemical signal appears. This signal grows when the electrode is modified with the nanomaterial (blue line), and the TDNs are immobilized over the sensing platform, as seen in the green line. Finally, the highest signal is obtained when the biosensing platform is challenged with the analyte, the BRCA1-C DNA sequence, complementary to the BRCA1 probe, as portrayed in the purple line. The observed process corroborates a catalytic process since the reduction peak disappears while the oxidation peak grows. A similar tendency is seen in Fig. 1B, which corresponds to the ECL signal of the different steps for biosensor development. As long as the electrochemical signal grows, the electrochemiluminescent signal also increases.

Raman spectroscopy was also carried out to characterize the biosensing platform. As shown in Fig. 2, the signal for CSPE shows significant signals for carbon at 1351 and 1579 $cm^{-1}$, respectively. These signals correspond to carbon's D and G bands [39]. Red line corresponds to the modified electrode CSPE/Graph-NS. The bands do not show a significant difference since the materials are identical. Finally, the blue line corresponds to the fully developed biosensor. Both D and G bands are observed, and signals corresponding to DNA appear, concrete bands at 353, 418, 889, and 964 $cm^{-1}$ for the DNA phosphate backbone and signals at 625 and 758 $cm^{-1}$ for adenine and cytosine, respectively [40].

Fig. 3 shows the topographical AFM characterization of CSPE (A), CSPE/Graph-NS (B), and CSPE/Graph-NS/TDN (C) on $SiO_2$. As expected, graphene sheets can be observed on the surface of the modified samples (images B and C).

Moreover, the biosensing platform was also characterized by SEM-EDAX. Fig. 4 shows SEM and EDAX characterization of CSPE (Fig. 4A and B), CSPE/Graph-NS (Fig. 4C and D) and CSPE/Graph-NS/TDN (Fig. 4E and F). Graphene sheets on the surface of CSPE can only be observed on the secondary electron SEM images of the modified CSPE samples (Fig. 4C and E). The corresponding back-scattered SEM images taken simultaneously are shown in Fig. S6 of the supporting information. The lack of contrast on those back-scattered images reveals that the materials within the image present similar atomic numbers and, therefore, equal components, as would be anticipated for CSPE and graphene. From the EDAX spectra analysis (Fig. 4B, D, and 4F), it can be concluded that the peaks corresponding to the phosphorus energy are only detected in the CSPE/Graph-NS/TDN sample. The presence of Phosphorus can be related to the existence of DNA.

**Table 3**
ECL and EQ DNA biosensors for BRCA1.

| Target analyte | Principle | Method | L.O.D | Reference |
|---|---|---|---|---|
| BRCA1 gene | PEP-PEDOT | DPV | 3.4 fM | [41] |
| | 3-QD@DNA | DPV | 1.20 aM | [42] |
| | DNA-mediated Au–Au dimer | SPC-ECL | 0.83 fM | [43] |
| | LNA modified TMSDR | ECL | 0.8 fM | [44] |
| | Graph-NS, CNDs and TDNs | ECL | 1.40 aM | This work |

Based on the obtained results, we can conclude that the biosensing platform has successfully developed.

The BRCA1 gene was detected by measuring the ECL signal catalyzed by carbon nanodots (CNDs) under optimal conditions. The final platform (CSPE/Graph-NS/TDN-BRCA1) was incubated with 10.0 μL of the analyte (BRCA1-C) at various concentrations (10.0 aM, 100 aM, 500 aM, 1.00 fM, 10.0 fM, 100 fM, 500 fM and 1.00 pM). After washing, the electrode was then treated with 60.0 μL of a solution containing $[Ru(bpy)_3]^{2+}$ and CNDs. The generated ECL signal corresponds to the ECL system in which $[Ru(bpy)_3]^{2+}$ is the luminophore and CNDs are the coreactants. As shown in Fig. 5A shows a linear relationship between the ECL signal and the logarithm of the analyte concentration, described by the equation (ECL Signal = 15.2·log[BRCA1] + 231; $R^2 = 0.99070$). This relationship was derived from the average of three measurements at each concentration. The sensitivity was 15.2 a.u. log($fM^{-1}$) with a coefficient of variation (CV) of 0.86 %. The limits of detection (LOD) and quantification (LOQ were determined using the blank signal and its standard deviation (Sb). By adding 3·Sb and 10·Sb to the blank signal and interpolating the obtained ECL Signal values on the calibration curve, the LOD and LOQ were calculated to be 1.41 aM and 7.50 aM, respectively.

To confirm the essential role of Graph-NS for the BRCA1 gene detection, ECL signal was measured for every step of the biosensor development without using graphene nanosheets. The obtained signal for every step is portrayed in Fig. S7, and the signal remains constant in each step. The ECL signals remain regular due to reactions between $[Ru(bpy)_3]^{2+}$ that has adsorbed non-specifically on the electrode surface and the co-reactant. Therefore, Graph-NS is necessary to anchor the nanotetrahedron upon the electrode surface and, afterward, carry out the biorecognition reaction to determine the analyte of interest.

The proposed biosensor has overcome general drawbacks that other biosensing platforms could not, including a lower LOD and LOQ, reported in the literature. Moreover, the linear range of the proposed biosensor is more comprehensive than the typical ones noted in the literature (see Table 3).

The selectivity of the biosensor was also assessed. ECL signal variation was studied for different samples containing 500 fM BRCA1-C in the presence and absence of a potential interferent, a non-complementary DNA sequence (BRCA1-NC), at the same concentration (500 fM). As it is shown in Fig. 5B, the variation of the ECL signal is minimal in the presence of the non-complementary strand. The stability of the biosensing platform was tested by measuring its response when stored at 4 °C over time. The results show that the initial recognition signal was kept at 92 % after 60 days (Fig. 5C).

Furthermore, clinical samples from breast cancer patients were examined to explore the potential for mutation detection in real DNA samples of the BRCA1 gene (Table 2). These samples were provided and validated by sequencing at La Paz Hospital. Two samples were used: one from a breast cancer patient (MUT) and another from a control patient (WT). As shown in Fig. 5D, the developed nanostructured bioconjugate can differentiate between mutated and control samples. Therefore, it can be concluded that the developed biosensor can detect a BRCA1 sequence from PCR clinical samples, moving towards the development of a simple, easy-to-use, and cost-effective point-of-care device.

Finally, in order to corroborate the advantages brought by the use of TDNs over the traditional single-strand probe technique, two studies were conducted. Firstly, as shown in Fig. S8A, the correlation between ECL signal and analyte concentration was evaluated for both strategies. Through the use of TDNs a lower LOD and LOQ and a higher sensitivity were obtained. Secondly, the single-base mutation was studied and shown in Fig. S8B. The use of TDNs allows for better recognition between the hybridization with the complementary strand and the mutated one than using a single-stranded probe.

## 4. Conclusions

A new electrochemiluminescent biosensor based on the combination of three different nanomaterials (Graph-NS, CNDs, and TDNs) has been developed and proved as a rapid, efficient, and easy-to-use alternative to detect a region of BRCA1 genome and also an insertion mutation on its code. CNDs allow ECL transduction using $[Ru(bpy)_3]^{2+}$ as the luminophore whereas Graph-NS allow the immobilization of aminated TDNs and the nanostructuring of the electrode. The developed biosensor can detect a specific region of the BRCA1 gene and mutations not only using synthetic DNA sequences, but also in human breast cancer patients' clinical samples.

## CRediT authorship contribution statement

**Daniel García-Fernández:** Writing – original draft, Investigation, Formal analysis. **Laura Gutiérrez-Gálvez:** Writing – original draft, Investigation, Formal analysis. **David López-Diego:** Writing – review & editing, Investigation, Formal analysis. **Mónica Luna:** Writing – review & editing, Supervision, Resources, Funding acquisition. **Íñigo Torres:** Writing – review & editing, Investigation, Formal analysis. **Félix Zamora:** Writing – review & editing, Supervision, Investigation, Funding acquisition. **Jesús Solera:** Writing – review & editing, Validation, Resources, Investigation. **Tania García-Mendiola:** Writing – review & editing, Writing – original draft, Supervision, Project administration, Methodology, Funding acquisition, Conceptualization. **Encarnación Lorenzo:** Writing – review & editing, Supervision, Investigation, Funding acquisition.

## Declaration of competing interest

The authors declare that they have no known competing financial interests or personal relationships that could have appeared to influence the work reported in this paper.

## Acknowledgements

The Spanish Ministry of Economy and Competitiveness has financially supported this work (PID2020-116728RB-I00, PID2023-150844OB-I00, RED2022-134120-T and TED2021-129738B–I00). Spanish Ministry of Universities supported Laura Gutiérrez-Gálvez with a FPU (FPU19/06309). European Union, through Autonomous Community of Madrid supported Daniel García-Fernández with a Programa Investigo grant in from the Plan de Recuperación, Transformación y Resiliencia– NextGenerationEU (09-PIN1-00013.4/2022-Puesto 83). The authors acknowledge the support of the EU and Horizon 2020 through Instruct Proposal PID: 21859, and the CRIOMECORR project (ESFRI-2019-01-CSIC-16) to the cryoEM CNB-CSIC facility. The authors also appreciate the service from the MiNa Laboratory at IMN, and funding from EU (FEDER, FSE), MINECO (project CSIC13-4E-1794) and CM (project S2018/NMT-4291 TEC2SPACE).

## Appendix A. Supplementary data

Supplementary data to this article can be found online at https://doi.org/10.1016/j.talanta.2024.127182.

## Data availability

Data will be made available on request.

## References

[1] R.L. Siegel, K.D. Miller, N.S. Wagle, A. Jemal, Cancer statistics, 2023, CA Cancer J Clin 73 (2023) 17–48, https://doi.org/10.3322/caac.21763.
[2] H. Sung, J. Ferlay, R.L. Siegel, M. Laversanne, I. Soerjomataram, A. Jemal, F. Bray, Global cancer statistics 2020: GLOBOCAN estimates of incidence and mortality

worldwide for 36 cancers in 185 countries, CA Cancer J Clin 71 (2021) 209–249, https://doi.org/10.3322/caac.21660.
[3] A. Ahmad (Ed.), Breast Cancer Metastasis and Drug Resistance, Springer International Publishing, Cham, 2019, https://doi.org/10.1007/978-3-030-20301-6.
[4] M. Senel, M. Dervisevic, F. Kokkokoğlu, Electrochemical DNA biosensors for label-free breast cancer gene marker detection, Anal. Bioanal. Chem. 411 (2019) 2925–2935, https://doi.org/10.1007/s00216-019-01739-9.
[5] M.P. Coleman, M. Quaresma, F. Berrino, J.-M. Lutz, R. De Angelis, R. Capocaccia, P. Baili, B. Rachet, G. Gatta, T. Hakulinen, A. Micheli, M. Sant, H.K. Weir, J. Mark Elwood, H. Tsukuma, S. Koifman, G. Azevedo Silva, S. Francisci, M. Santaquilani, A. Verdecchia, H.H. Storm, J.L. Young, The CONCORD Working Group, Cancer survival in fi ve continents: a worldwide population-based study (CONCORD), Oncology 9 (2008), https://doi.org/10.1016/S1470. Www.Thelancet.Com.
[6] S. Ranjbari, M. Rezayi, R. Arefinia, S.H. Aghaee-Bakhtiari, B. Hatamluyi, A. Pasdar, A novel electrochemical biosensor based on signal amplification of Au HFGNs/PnBA-MXene nanocomposite for the detection of miRNA-122 as a biomarker of breast cancer, Talanta 255 (2023), https://doi.org/10.1016/j.talanta.2022.124247.
[7] M. Garg, A.L. Sharma, S. Singh, Advancement in biosensors for inflammatory biomarkers of SARS-CoV-2 during 2019–2020, Biosens. Bioelectron. 171 (2021), https://doi.org/10.1016/j.bios.2020.112703.
[8] H. Ehzari, M. Safari, M. Samimi, Signal amplification of novel sandwich-type genosensor via catalytic redox-recycling on platform MWCNTs/Fe3O4@TMU-21 for BRCA1 gene detection, Talanta 234 (2021), https://doi.org/10.1016/j.talanta.2021.122698.
[9] M. Pirsaheb, S. Mohammadi, R. Khodarahmi, Z. Hoseinkhani, K. Mansouri, M. Payandeh, A turn off fluorescence probe based on carbon dots for highly sensitive detection of BRCA1 gene in real samples and cellular imaging, J. Fluoresc. 32 (2022) 1733–1741, https://doi.org/10.1007/s10895-022-02954-x.
[10] Q. Hu, J. Wan, Y. Luo, S. Li, X. Cao, W. Feng, Y. Liang, W. Wang, L. Niu, Electrochemical detection of femtomolar DNA via boronate affinity-mediated decoration of polysaccharides with electroactive tags, Anal. Chem. 94 (2022) 12860–12865, https://doi.org/10.1021/acs.analchem.2c02894.
[11] J. Zhang, S. Arbault, N. Sojic, D. Jiang, Electrochemiluminescence imaging for bioanalysis, Annual Review of Analytical Chemistry Annu. Rev. Anal. Chem. 14 (2019) 17–18, https://doi.org/10.1146/annurev-anchem-061318, n.d.
[12] Z. Liu, W. Qi, G. Xu, Recent advances in electrochemiluminescence, Chem. Soc. Rev. 44 (2015) 3117–3142, https://doi.org/10.1039/c5cs00086f.
[13] X. Ma, W. Gao, F. Du, F. Yuan, J. Yu, Y. Guan, N. Sojic, G. Xu, Rational design of electrochemiluminescent devices, Acc. Chem. Res. 54 (2021) 2936–2945, https://doi.org/10.1021/acs.accounts.1c00230.
[14] L. Gutiérrez-Gálvez, T. García-Mendiola, C. Gutiérrez-Sánchez, T. Guerrero-Esteban, C. García-Diego, I. Buendía, M.L. García-Bermejo, F. Pariente, E. Lorenzo, Carbon nanodot–based electrogenerated chemiluminescence biosensor for miRNA-21 detection, Microchim. Acta 188 (2021), https://doi.org/10.1007/s00604-021-05038-y.
[15] Y.M. Long, L. Bao, J.Y. Zhao, Z.L. Zhang, D.W. Pang, Revealing carbon nanodots as coreactants of the anodic electrochemiluminescence of Ru(bpy)32+, Anal. Chem. 86 (2014) 7224–7228, https://doi.org/10.1021/ac502405p.
[16] V.C. Tsafack, C.A. Marquette, B. Leca, L.J. Blum, An electrochemiluminescence-based fibre optic biosensor for choline flow injection analysis, Analyst 125 (2000) 151–155, https://doi.org/10.1039/a907709j.
[17] W. Miao, Electrogenerated chemiluminescence and its biorelated applications, Chem Rev 108 (2008) 2506–2553, https://doi.org/10.1021/cr068083a.
[18] L. Hai-Juan, H. Shuang, H. Lian-Zhe, X. Guo-Bao, Progress in Ru(bpy)32+ electrogenerated chemiluminescence, Fenxi Huaxue/Chin. J. Anal. Chem. 37 (2009) 1557–1565, https://doi.org/10.1016/S1872-2040(08)60139-5.
[19] N. Kottam, S.P. Smrithi, Luminescent carbon nanodots: current prospects on synthesis, properties and sensing applications, Methods Appl. Fluoresc. 9 (2021), https://doi.org/10.1088/2050-6120/abc008.
[20] Y. Xu, J. Liu, C. Gao, E. Wang, Applications of carbon quantum dots in electrochemiluminescence: a mini review, Electrochem. Commun. 48 (2014) 151–154, https://doi.org/10.1016/j.elecom.2014.08.032.
[21] N.M.R. Peres, R.M. Ribeiro, Focus on graphene, New J. Phys. 11 (2009), https://doi.org/10.1088/1367-2630/11/9/095002.
[22] F. Catania, E. Marras, M. Giorcelli, P. Jagdale, L. Lavagna, A. Tagliaferro, M. Bartoli, A review on recent advancements of graphene and graphene-related materials in biological applications, Appl. Sci. 11 (2021) 1–21, https://doi.org/10.3390/app11020614.
[23] C.E. Junkermeier, D. Solenov, T.L. Reinecke, Adsorption of NH2 on graphene in the presence of defects and adsorbates, J. Phys. Chem. C 117 (2013) 2793–2798, https://doi.org/10.1021/jp309419x.
[24] P.W.K. Rothemund, Folding DNA to create nanoscale shapes and patterns, Nature 440 (2006) 297–302, https://doi.org/10.1038/nature04586.
[25] P.L. Xavier, A.R. Chandrasekaran, DNA-Based Construction at the Nanoscale: Emerging Trends and Applications, 2018.
[26] L. Qian, E. Winfree, Scaling up digital circuit computation with DNA strand displacement cascades, Science 332 (2011) 1196–1201, https://doi.org/10.1126/science.1200520, 1979.
[27] Z. Ge, M. Lin, P. Wang, H. Pei, J. Yan, J. Shi, Q. Huang, D. He, C. Fan, X. Zuo, Hybridization chain reaction amplification of microRNA detection with a tetrahedral DNA nanostructure-based electrochemical biosensor, Anal. Chem. 86 (2014) 2124–2130, https://doi.org/10.1021/ac4037262.
[28] I. Horcas, R. Fernández, J.M. Gómez-Rodríguez, J. Colchero, J. Gómez-Herrero, A. M. Baro, WSXM: a software for scanning probe microscopy and a tool for nanotechnology, Rev. Sci. Instrum. 78 (2007) 013705, https://doi.org/10.1063/1.2432410.
[29] L. Gutiérrez-Gálvez, R. del Caño, I. Menéndez-Luque, D. García-Nieto, M. Rodríguez-Peña, M. Luna, T. Pineda, F. Pariente, T. García-Mendiola, E. Lorenzo, Electrochemiluminescent nanostructured DNA biosensor for SARS-CoV-2 detection, Talanta 240 (2022) 123203, https://doi.org/10.1016/j.talanta.2021.123203.
[30] L. Gutiérrez-Gálvez, M.V. Sulleiro, C. Gutiérrez-Sánchez, D. García-Nieto, M. Luna, E.M. Pérez, T. García-Mendiola, E. Lorenzo, MoS2-Carbon nanodots as a new electrochemiluminescence platform for breast cancer biomarker detection, Biosensors 13 (2023) 348, https://doi.org/10.3390/bios13030348.
[31] Y.-M. Long, L. Bao, J.-Y. Zhao, Z.-L. Zhang, D.-W. Pang, Revealing carbon nanodots as coreactants of the anodic electrochemiluminescence of Ru(bpy) $_{32+}$, Anal. Chem. 86 (2014) 7224–7228, https://doi.org/10.1021/ac502405p.
[32] L.M. Malard, M.A. Pimenta, G. Dresselhaus, M.S. Dresselhaus, Raman spectroscopy in graphene, Phys. Rep. 473 (2009) 51–87, https://doi.org/10.1016/j.physrep.2009.02.003.
[33] Z. Li, B. Zhao, D. Wang, Y. Wen, G. Liu, H. Dong, S. Song, C. Fan, DNA nanostructure-based universal microarray platform for high-efficiency multiplex bioanalysis in biofluids, ACS Appl. Mater. Interfaces 6 (2014) 17944–17953, https://doi.org/10.1021/am5047735.
[34] N. Mitchell, R. Schlapak, M. Kastner, D. Armitage, W. Chrzanowski, J. Riener, P. Hinterdorfer, A. Ebner, S. Howorka, A DNA nanostructure for the functional assembly of chemical groups with tunable stoichiometry and defined nanoscale geometry, Angewandte Chemie - International Edition 48 (2009) 525–527, https://doi.org/10.1002/anie.200804264.
[35] Y. Wen, H. Pei, Y. Wan, Y. Su, Q. Huang, S. Song, C. Fan, DNA nanostructure-decorated surfaces for enhanced aptamer-target binding and electrochemical cocaine sensors, Anal. Chem. 83 (2011) 7418–7423, https://doi.org/10.1021/ac201491p.
[36] Y. Wen, H. Pei, Y. Shen, J. Xi, M. Lin, N. Lu, X. Shen, J. Li, C. Fan, DNA Nanostructure-based Interfacial engineering for PCR-free ultrasensitive electrochemical analysis of microRNA, Sci. Rep. 2 (2012), https://doi.org/10.1038/srep00867.
[37] R. Kalendar, D. Lee, A.H. Schulman, FastPCR software for PCR primer and probe design and repeat search. https://www.researchgate.net/publication/284652273, 2009.
[38] H. Pei, N. Lu, Y. Wen, S. Song, Y. Liu, H. Yan, C. Fan, A DNA nanostructure-based biomolecular probe carrier platform for electrochemical biosensing, Adv. Mater. 22 (2010) 4754–4758, https://doi.org/10.1002/adma.201002767.
[39] * M.A. Pimenta, G. Dresselhaus, M.S. Dresselhaus, L.G. Cançado, A. Jorio, R. Saito, Studying disorder in graphite-based systems by Raman spectroscopy, Phys. Chem. Chem. Phys. 9 (2007) 1276–1291, https://doi.org/10.1039/b613962k.
[40] B Prescott, Steinmetz, GJ Thomas Jr., Characterization of DNA structures by laser Raman spectroscopy, Biopolymers 23 (2) (1984 Feb) 235–256, https://doi.org/10.1002/bip.360230206. PMID: 6704487.
[41] Y. Wang, F. Wang, Z. Han, K. Huang, X. Wang, Z. Liu, S. Wang, Y. Lu, Construction of sandwiched self-powered biosensor based on smart nanostructure and capacitor: toward multiple signal amplification for thrombin detection, Sens Actuators B Chem 304 (2020), https://doi.org/10.1016/j.snb.2019.127418.
[42] B. Yang, S. Zhang, X. Fang, J. Kong, Double signal amplification strategy for ultrasensitive electrochemical biosensor based on nuclease and quantum dot-DNA nanocomposites in the detection of breast cancer 1 gene mutation, Biosens. Bioelectron. 142 (2019), https://doi.org/10.1016/j.bios.2019.111544.
[43] Q. Ma, Q. Zhang, Y. Tian, Z. Liang, Z. Wang, S. Xu, DNA-mediated au-au dimer-based surface plasmon coupling electrochemiluminescence sensor for BRCA1 gene detection, Anal. Chem. 93 (2021) 3308–3314, https://doi.org/10.1021/acs.analchem.0c05440.
[44] X. Zhang, J. Zhang, D. Wu, Z. Liu, S. Cai, M. Chen, Y. Zhao, C. Li, H. Yang, J. Chen, Ultraselective electrochemiluminescence biosensor based on locked nucleic acid modified toehold-mediated strand displacement reaction and junction-probe, Analyst 139 (2014) 6109–6112, https://doi.org/10.1039/c4an01363h.